NASA TECHNICAL NOTE

NASA TN D-4516

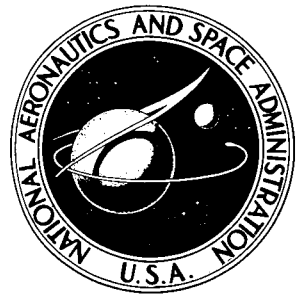

NASA TN D-4516

COLLISIONLESS CYLINDRICAL DIODE

by Charles M. Goldstein

Lewis Research Center

Cleveland, Ohio

NATIONAL AERONAUTICS AND SPACE ADMINISTRATION • WASHINGTON, D. C. • APRIL 1968

NASA TN D-4516

COLLISIONLESS CYLINDRICAL DIODE

By Charles M. Goldstein

Lewis Research Center
Cleveland, Ohio

NATIONAL AERONAUTICS AND SPACE ADMINISTRATION

For sale by the Clearinghouse for Federal Scientific and Technical Information
Springfield, Virginia 22151 – CFSTI price $3.00

COLLISIONLESS CYLINDRICAL DIODE

by Charles M. Goldstein

Lewis Research Center

SUMMARY

A complete formulation and numerical results for the collisionless space-charge problem of a cylindrical diode with thermionically emitted electrons are presented. This formulation allows calculation of the current-voltage characteristics from the Schottky retarding region to saturation. In addition, the onset of the Schottky retarding region is unambiguously defined.

INTRODUCTION

The study of collisionless electron flow in cylindrical geometries has a long history; a review of these studies is to be found in the article by Ivey (ref. 1). Except for the studies of Wheatcroft (1940, ref. 2) and Schottky (1914, ref. 3), the early studies involved broad idealized assumptions such as monoenergetic electron emission and virtual cathodes at the potential minimum.

Schottky (ref. 3) derived an expression for the current-voltage characteristic in the retarding potential range, that is, for cases where the potential is monotonically decreasing. He assumed, however, that his relation was valid for all monotonically retarding potentials. It will be shown in this report that there exists, in general, a range of collector potentials associated with monotonically retarding potentials for which Schottky's relation is not valid. In his defense, however, let it be noted that this potential range becomes negligible for large ratios of collector radius to emitter radius (e.g., filament emitters).

Wheatcroft (ref. 2) succeeded in obtaining numerical solutions to the mathematical equations over a limited range of collector potentials. These solutions were obtained by laborious numerical calculations before the advent of the high speed electronic computer. He was forced, therefore, to employ some approximate methods of solution which unfortunately hid some of the physical aspects in the range he treated. Because of this limitation, numerical solutions for the cylindrical diode from the Schottky retarding regime

to saturation have never been obtained. This report is an attempt to fill the void. We are more fortunate than Dr. Wheatcroft in the availability of high speed electronic computers.

Because the wide spread availability of computers today provides the means of calculating diode characteristics for all collector potentials of interest, it will not be necessary, as in previous studies (refs. 2 and 4), to concern ourselves with the position and magnitude of the potential minimum in the space-charge-limited cases. Meaningful to the experimentalist are the parameters he can control and the variables which he can observe. Among the former are emitter radius, temperature, work function, collector radius, and collector potential. The easiest (and often times the only) variable he can measure is the current to the collector. It is therefore somewhat artificial to present theoretical results in terms of the position and magnitude of the potential minimum. For given physical diode characteristics, it is, furthermore, easy to investigate the theoretical variation of the potential minimum by numerical solutions.

ANALYSIS

An investigation of the characteristics of the collisionless cylindrical diode from the Schottky retarding region (hereinafter SRR) to saturation is presented. SRR is defined as that region in which the Schottky relation (ref. 3)

$$\frac{I}{I_o} = ae^{\varphi}\operatorname{erf}\left(\frac{\sqrt{\lambda\varphi}}{a}\right) + \operatorname{erfc}\left(\sqrt{\lambda\varphi}\right) \tag{1}$$

is valid. In equation (1),

$$a \equiv \frac{r_c}{r_o} \tag{2}$$

$$\lambda \equiv \frac{-1}{1 - a^{-2}}$$

$$\varphi \equiv -\frac{V}{kT} \tag{3}$$

r_o and r_c are the emitter and collector radii, respectively, V is the potential energy (not just potential) of an electron in the electrostatic field of the diode, T is the emitter temperature, k is the Boltzmann constant, and φ is the dimensionless electrostatic potential. (All symbols are defined in appendix A.)

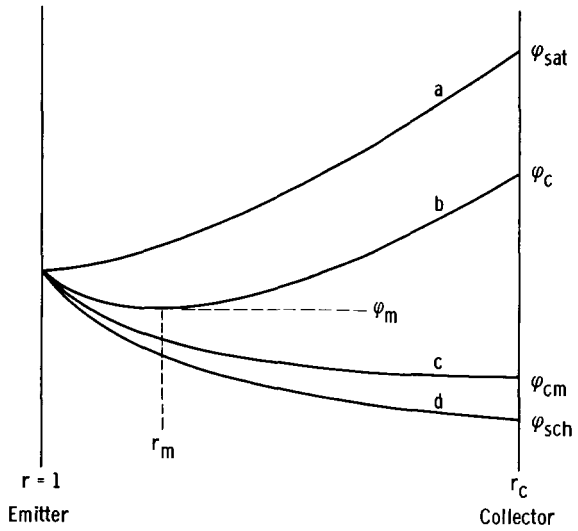

Figure 1. - Space-charge potentials.

Physically, SRR denotes a region wherein the current to the collector is a function of the collector potential only and not of the functional form of the potential in the interelectrode space. In the planar case (ref. 5), the onset of SRR corresponds to the onset of a monotonically retarding potential. In general, this correspondence is not true in the cylindrical case; that is, there may be monotonically retarding potentials for which the electron current to the collector is not a function of the collector potential alone.

Characteristic potentials (and their corresponding collector potential) for the cylindrical diode are shown in figure 1. Here the dimensionless radius r is defined as $\hat{r}/\hat{r}_0$. In general, the potential signaling the onset of SRR lies below that of the first monotonically decreasing potential, as shown by curves c and d, respectively. Curve b depicts a typical space-charge potential and curve a signals the onset of saturation current to the collector. Curve a is identified by zero potential slope at the emitter, while curve c is identified by zero potential slope at the collector.

The problem is to find self-consistent solutions to Poisson's equation which, for the cylindrical diode, can be expressed in the form (derived in appendix B)

$$\varphi''(\xi) = B_0 e^{2\xi} n(\xi, \varphi) \tag{B14}$$

where

$$\xi \equiv \ln r \tag{B13}$$

the space-charge parameter B_0 (mks units) is given by

$$B_o \equiv \frac{e^2 n_o r_o^2}{\epsilon_o kT} \tag{B12}$$

and $n(\xi, \varphi)$ represents the dimensionless electron density.

With the assumption that the emitted electrons have a half-Maxwellian velocity distribution and encounter no collisions, formal expressions for the electron density $n(\xi, \varphi)$ as a function of radius and potential are derived in appendixes B to D. These expressions for the density become quite complex because of the exchange between radial angular momentum in cylindrical geometries. This exchange can be clarified by a description of the possible electron trajectories in terms of an equivalent one-dimensional potential energy.

Equivalent One-Dimensional Potential Energies

The sum of the radial and tangential energy components of an electron at radius $\hat{r}$ may be expressed by

$$\frac{1}{2} m\hat{u}^2 + V(\hat{r}) + \frac{L^2}{2m\hat{r}^2} \tag{4}$$

where L is the angular momentum. (Here dimensional variables are used for heuristic reasons.) Since this sum is a constant of the motion,

$$\frac{1}{2} m\hat{u}^2 + V(\hat{r}) + \frac{L^2}{2m\hat{r}^2} = \frac{1}{2} m\hat{u}_o^2 + \frac{L^2}{2m\hat{r}_o^2} \tag{5}$$

where, for convenience, $V(\hat{r}_o)$ is taken to be 0. A new constant of motion E will now be defined by adding $-L^2/2m\hat{r}_o^2$ to both sides of equation (5):

$$E \equiv \frac{1}{2} m\hat{u}^2 + V(\hat{r}) + \frac{L^2}{2m}\left(\frac{1}{\hat{r}^2} - \frac{1}{\hat{r}_o^2}\right) = \frac{1}{2} m\hat{u}_o^2 \tag{6}$$

Note that E is equivalent to the radial kinetic energy of emission. Now, as in reference 6, an equivalent one-dimensional potential energy (hereinafter EODP) $\tilde{V}$ can be defined as

$$\tilde{V}(\hat{r}) \equiv V(\hat{r}) + \frac{L^2}{2m}\left(\frac{1}{\hat{r}^2} - \frac{1}{\hat{r}_o^2}\right) = V(\hat{r}) + V_L(\hat{r}) \tag{7}$$

where the force on the equivalent particle is given by $-d\tilde{V}/d\hat{r}$. The "angular potential energy" $V_L(\hat{r})$ represents the contribution of angular motion to $\tilde{V}(\hat{r})$. The potential energies $V(\hat{r})$, $V_L(\hat{r})$, and $\tilde{V}(\hat{r})$ are shown in figure 2 for a typical space-charge con-

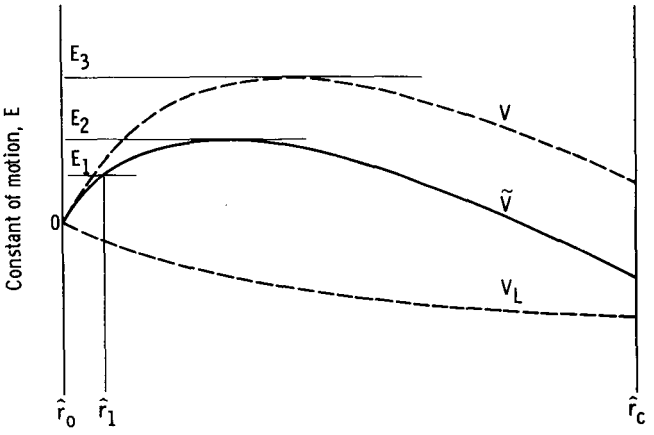

Figure 2. - Equivalent one-dimensional potential for cylindrical diode.

dition. Here, $V(\hat{r})$ has the form of a potential energy barrier in front of the emitter, while $V_L(\hat{r})$ has the form of a potential energy sink. Their sum, $\tilde{V}(\hat{r})$, also has the form of a potential barrier in front of the emitter, but its maximum is much less than that corresponding to $V(\hat{r})$. By referring again to $\tilde{V}(\hat{r})$, it can be observed that only electrons with $E > E_2$ can "escape" the emitter and reach the collector. This is in contrast to the planar geometry where E must be greater than E_3 for the electron to reach the collector. An electron with $E = E_1 < E_2$ will reach a radius $\hat{r}_1$ before returning to the emitter.

Qualitative characteristics of the different EODP appearing in the analysis of the cylindrical diode space-charge problem are shown in figures 3 and 4. In these figures, the potential energy $V(\hat{r})$ is a characteristic of the diode operating condition, while $V_L(\hat{r})$ is the angular potential energy of a particular electron. In other words, the whole spectrum of angular potential energies is present at any given time since $V_L(\hat{r}) \propto L^2 = \hat{r}_o^2\hat{v}_o^2$, where $\hat{v}_o$ is the tangential electron emission velocity. For obvious reasons of clarity, only one $V_L(\hat{r})$ is depicted in each case. Since the different EODP depend on the functional form of $V(\hat{r})$, not all the types shown in figures 3 and 4 can exist at one time.

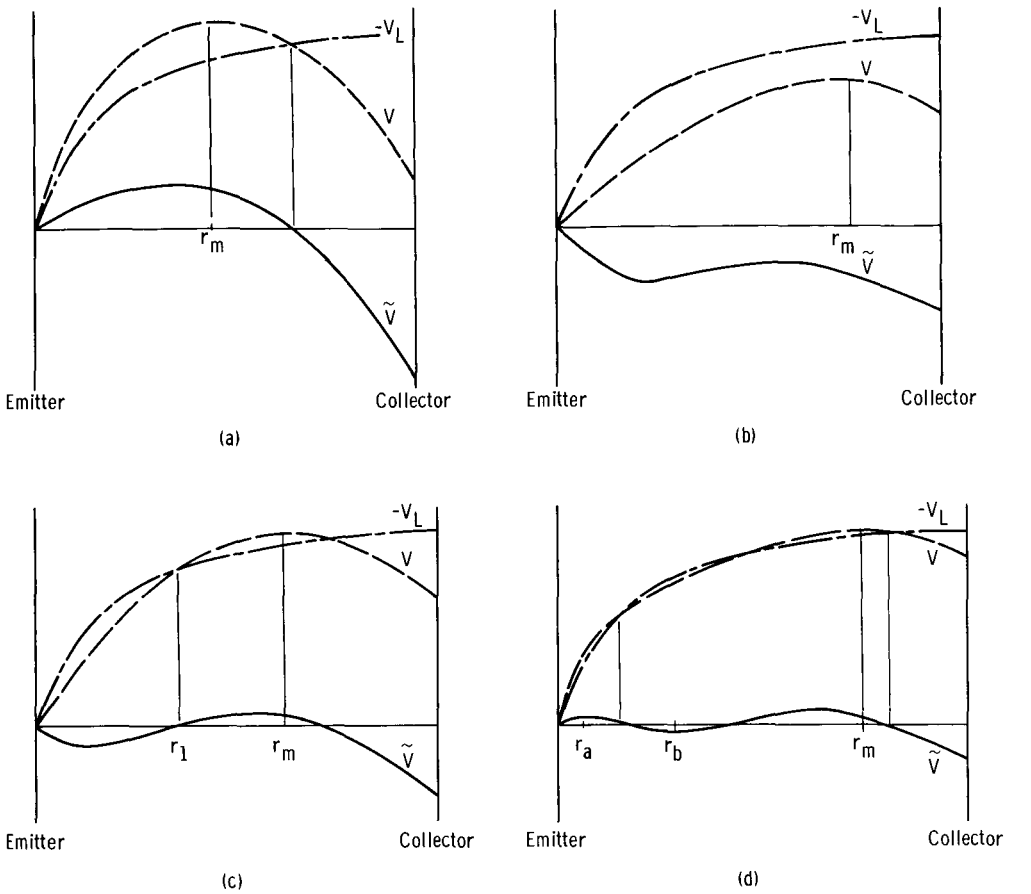

Figure 3. - Types of equivalent one-dimensional potentials for cylindrical diode with potential maximum (r_m is position at potential maximum).

In figure 3(a) only those electrons for which E is greater than the maximum $\tilde{V}$ (hereinafter $\tilde{V}_{max}$) will reach the collector. The EODP of figure 3(b) allows all electrons to reach the collector regardless of E (even electrons for which $E = 1/2\ mu_o^2 = 0$). Electrons for which the EODP is as that depicted in figure 3(c) will reach r_1 regardless of E, but will reach the collector only for $E > \tilde{V}_{max}$. In figure 3(d), two maximums occur in $\tilde{V}$. Electrons for which E is greater than the first $\tilde{V}_{max}$ may still be returned to the emitter if E is not simultaneously greater than the second $\tilde{V}_{max}$.

Three other EODP are shown in figure 4 for the case of a monotonically retarding potential energy. The interpretations of the three different EODP are the same as in figure 3. Figure 4 is important because it clarifies the definition of the Schottky retarding region (SRR). As previously defined, SRR occurs when the electron current to the collector is a function of the collector potential only. It has been observed that an electron cannot reach the collector unless it has an $E > \tilde{V}_{max}$. Hence, the SRR is defined by those potential energies V such that for all V_L, $\tilde{V}_{max}$ occurs at the collector.

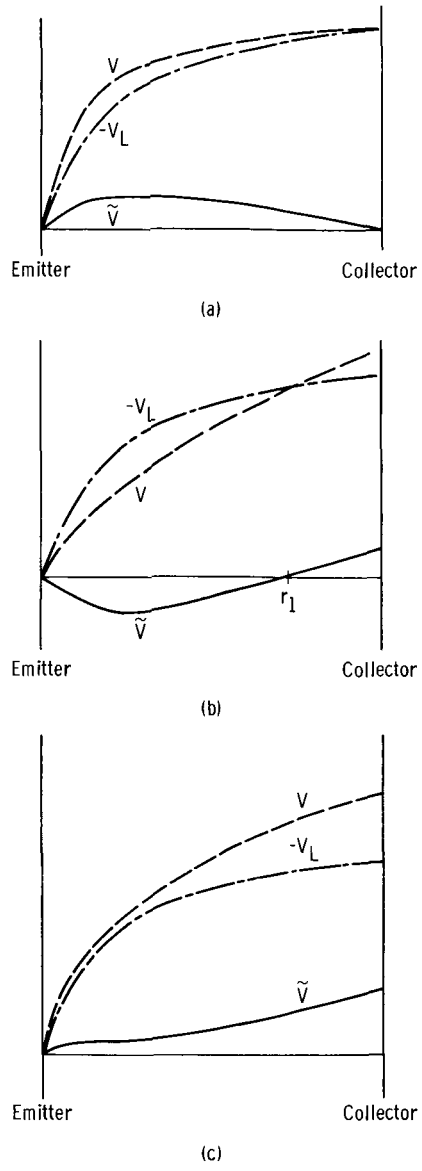

Figure 4. - Types of equivalent one-dimensional potentials for cylindrical diode with monotonic potential.

Figure 4(a) shows that this condition is not always satisfied by a monotonically retarding potential energy.

As shown in appendix B, Wheatcroft (ref. 2) implicitly recognized only that condition depicted in figure 3(a). A complete formulation of the collisionless electron space-charge problem embodying all the trajectories is given in appendixes B to D.

DISCUSSION

In the absence of space charge, the current-voltage curves would coincide with the Schottky curves (defined by eq. (1)) in the retarding region (fig. 5). For $r_c/r_o = 1$ ($\ln r_c/r_o = 0$), the Schottky curve is simply the Maxwell-Boltzmann line associated with the planar diode. The current-voltage curves with space charge present are shown in figure 6 for various values of $\ln r_c/r_o$ and B_o (defined in eq. (B12)).

For given $\ln r_c/r_o$, increasing B_o results in a larger saturation potential and a decrease in I/I_o for a fixed collector potential. A similar observation is valid if B_o is given and $\ln r_c/r_o$ is allowed to increase.

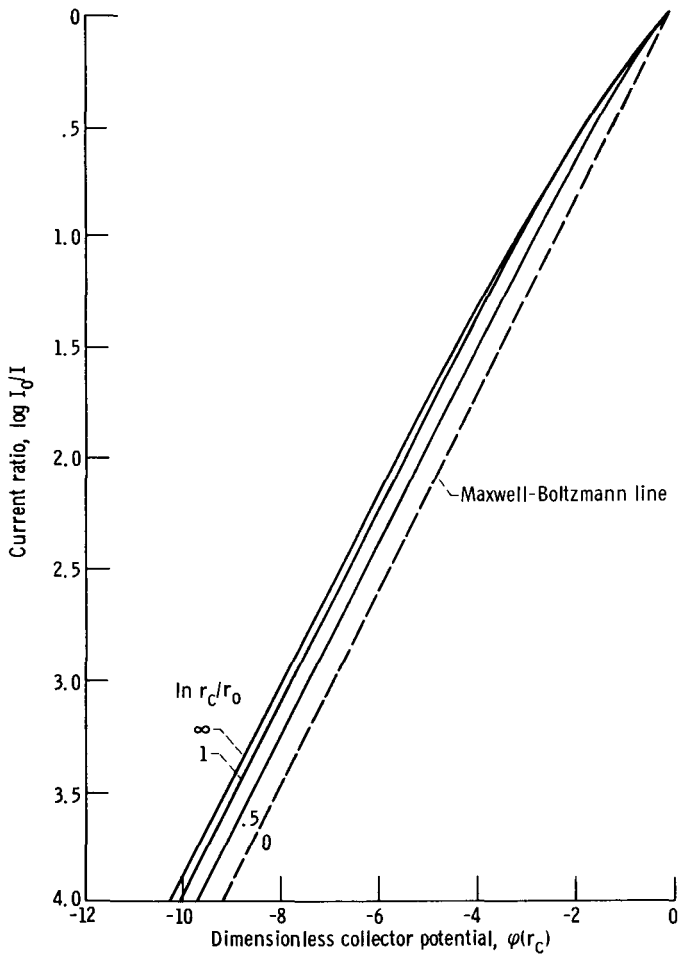

Figure 5. - Schottky curves.

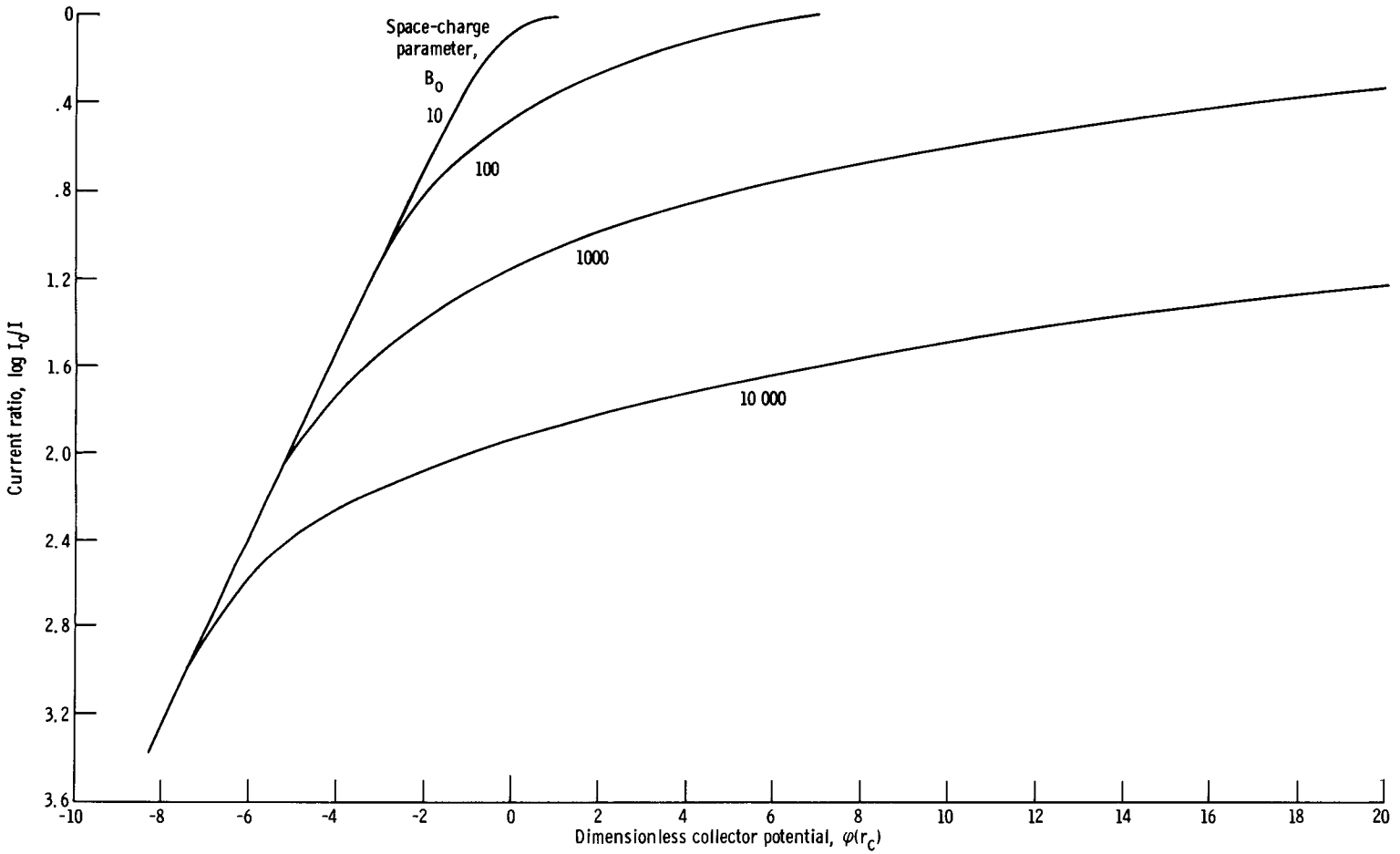

(a) In $r_c/r_0 = 0.5$.

Figure 6. - Current-voltage curves.

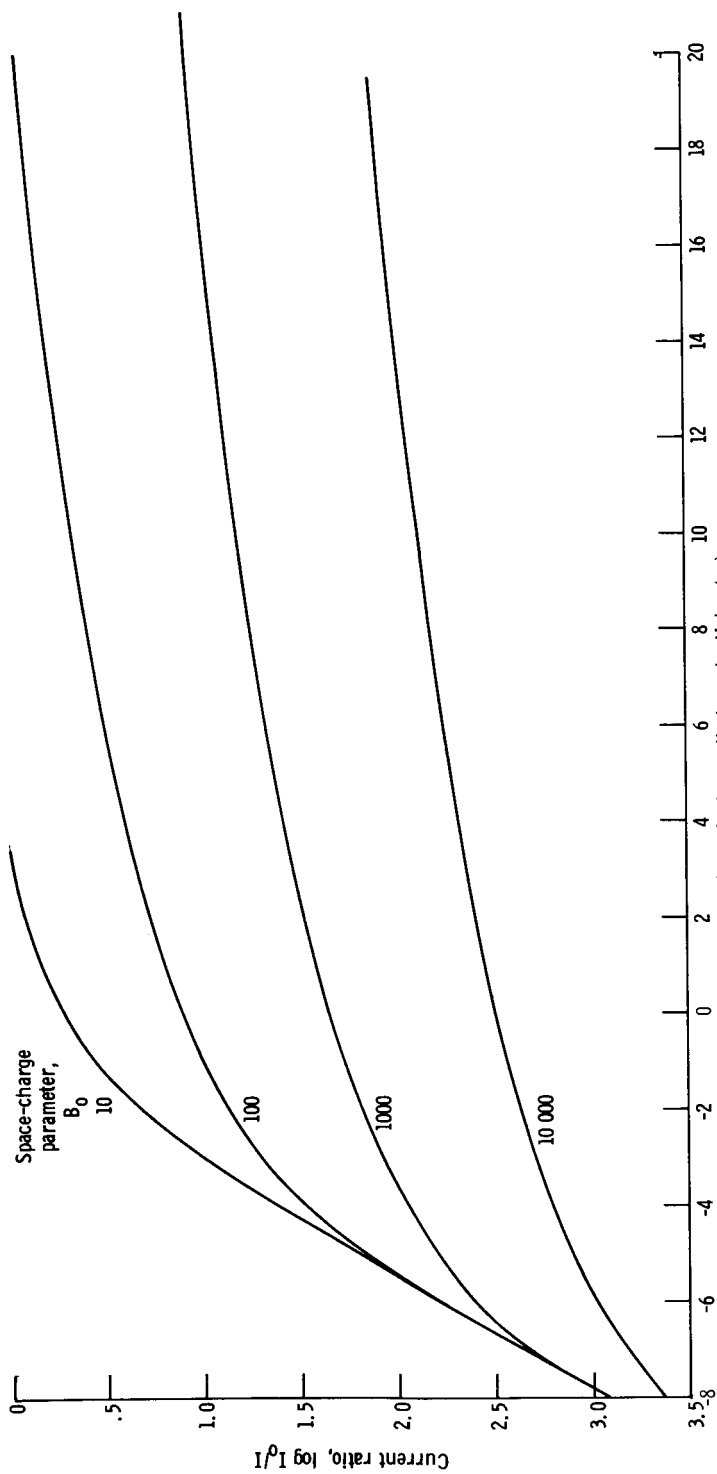

(b) ln $r_c/r_0 = 1$.

Figure 6. - Continued.

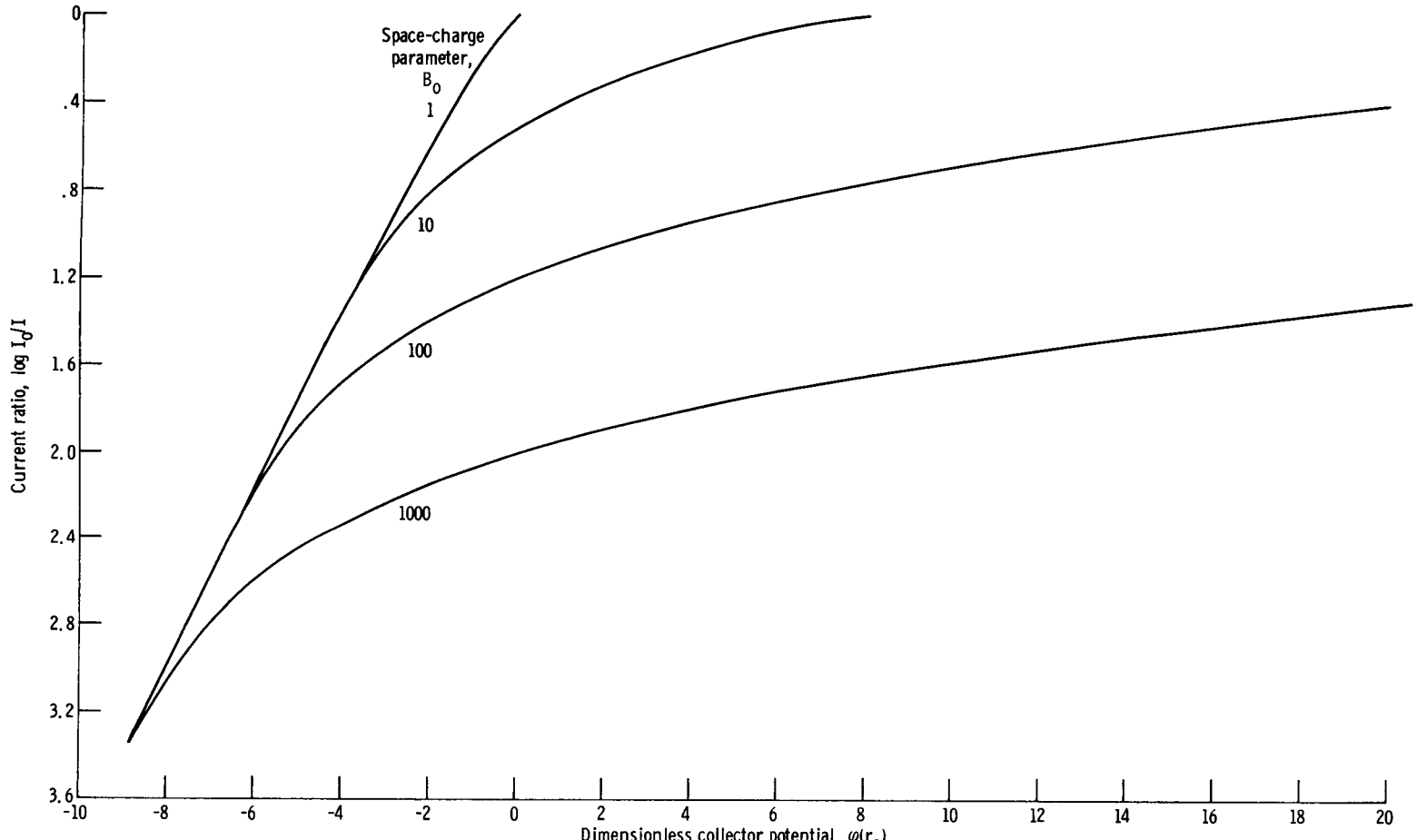

(c) In $r_c/r_0 = 1.5$.

Figure 6. - Continued.

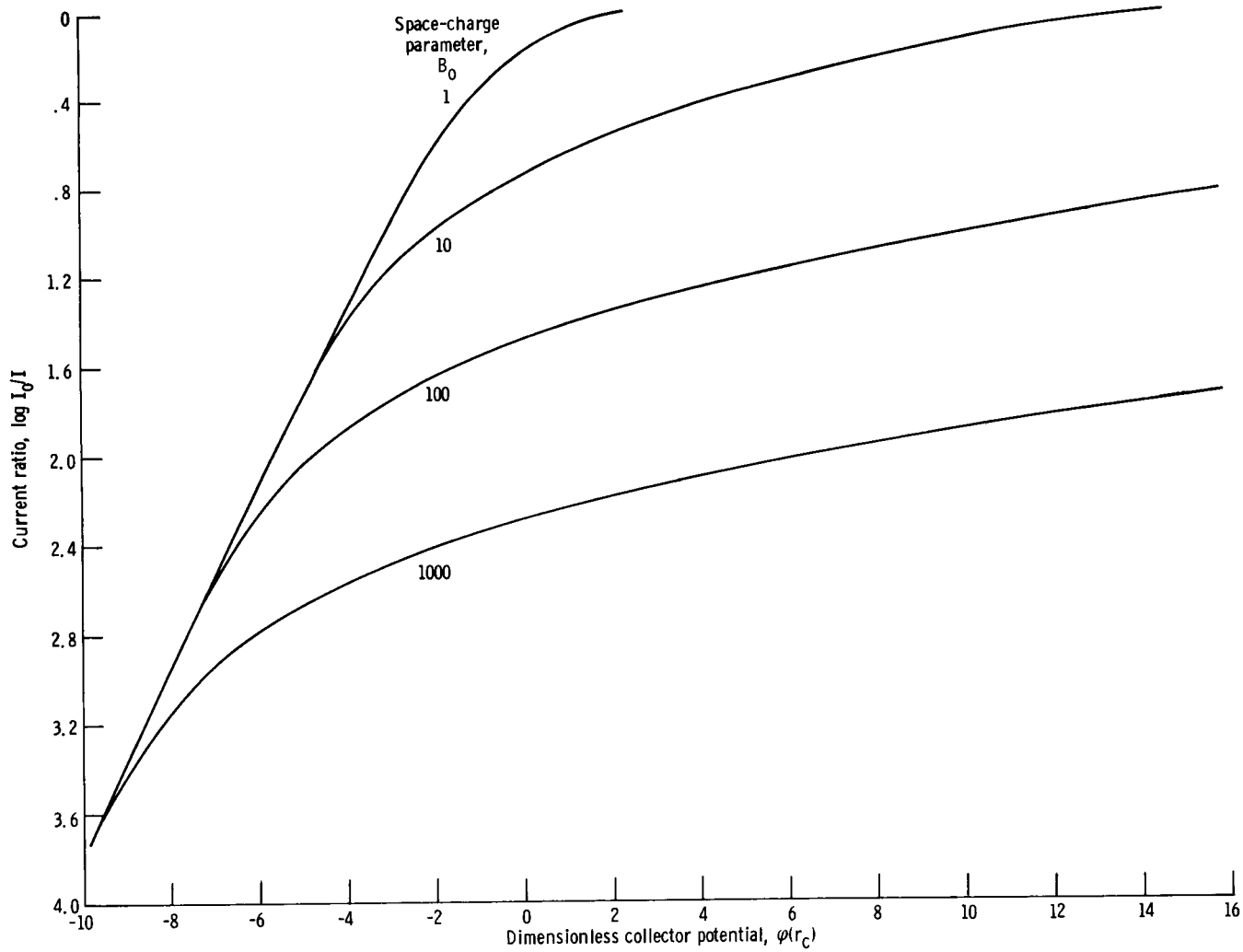

(d) In $r_c/r_o = 2$.

Figure 6. - Continued.

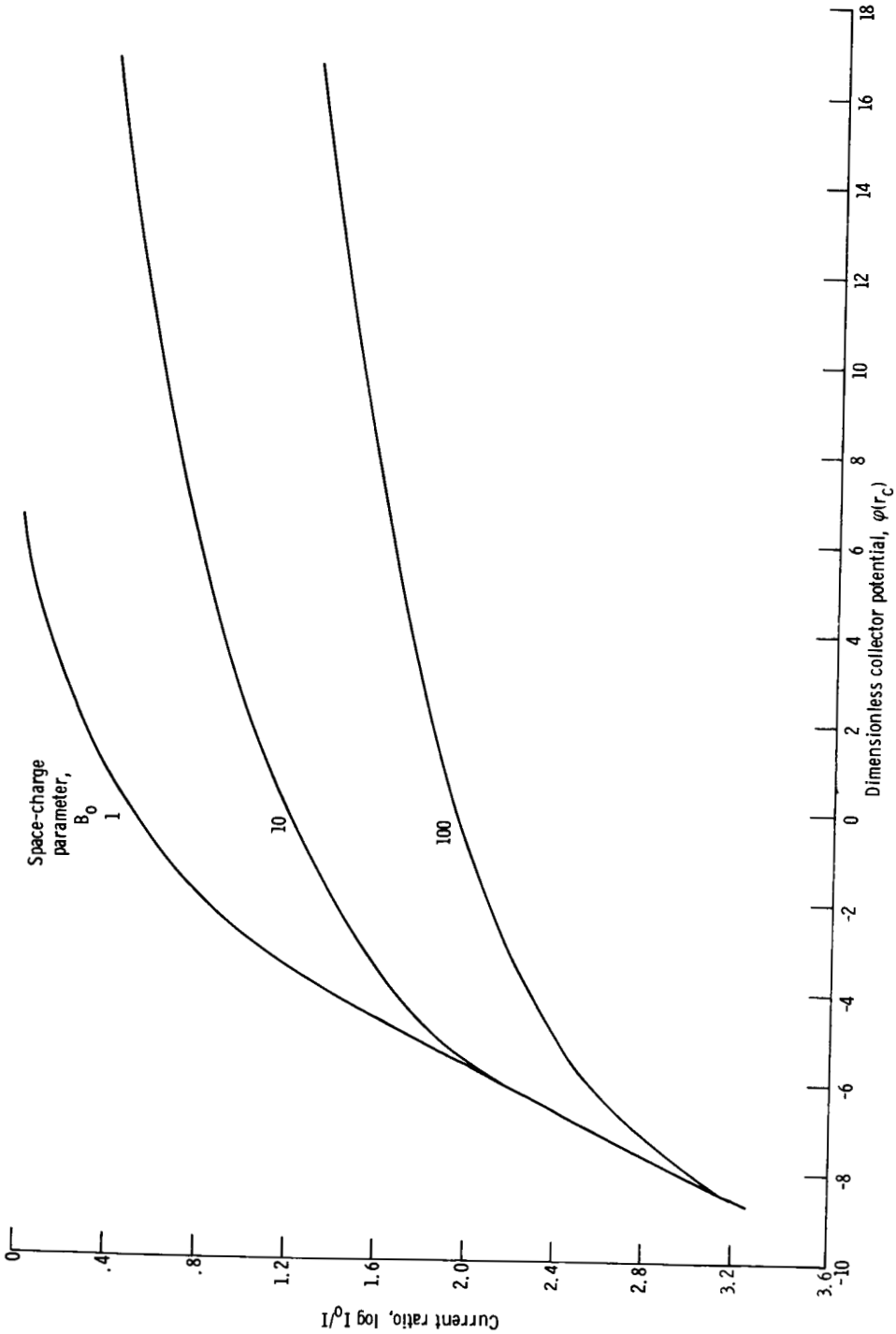

(e) In $r_c/r_0 = 3$.

Figure 6. - Concluded.

As mentioned in the INTRODUCTION, the onset of the SRR does not coincide, in general, with the onset of monotonic retarding potentials. Figure 7 demonstrates this fact quantitatively. The solid lines in this figure are simply the Schottky curves of figure 5 plotted against a different abscissa to effect a better separation. The dashed lines indicate the locus of points where the potential first becomes monotonic for the indicated values of B_o. The dot-dash lines represent the locus of points signaling the onset of the SRR for the indicated values of B_o. Here it is also apparent that the two lines coalesce into one as r_c/r_o gets very large.

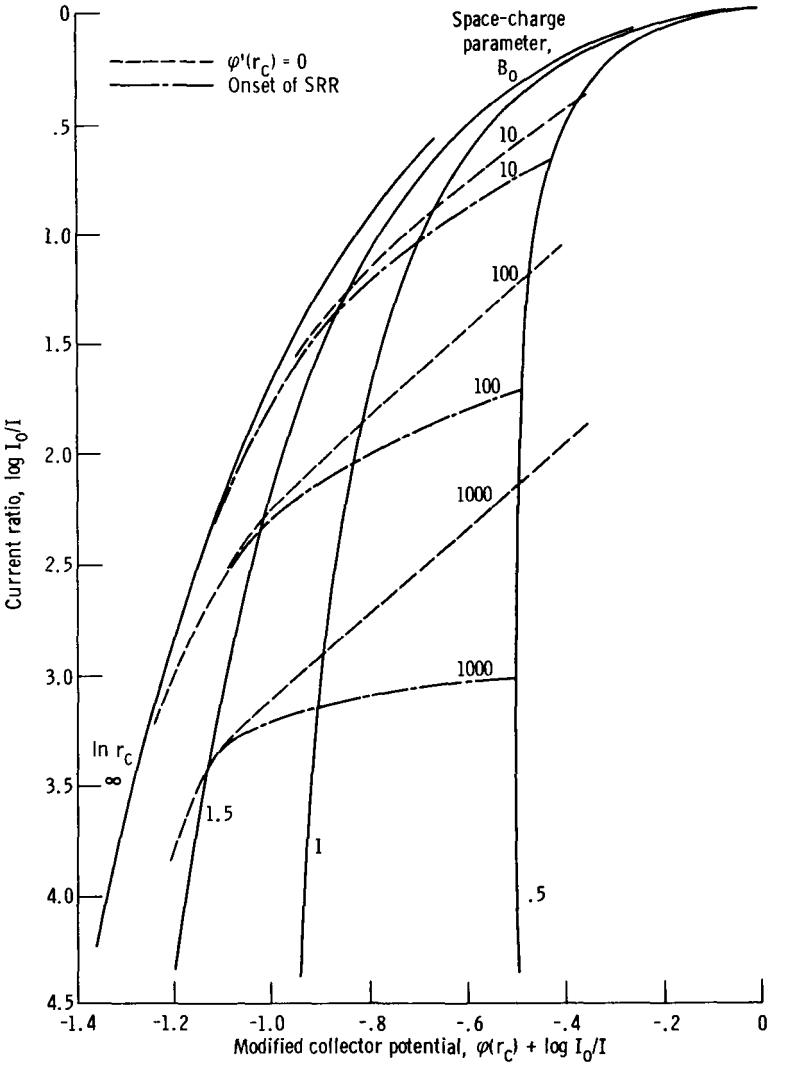

Figure 7. - Limits on Schottky curve.

Comparisons of the theoretical results with some experimental results are given in figure 8. (The abscissas have been corrected for the experimentally determined contact potential $\Delta\varphi$.) The experimental results in figure 8 were reported by Schottky (ref. 3) in 1914. The theoretical curves of figure 8 were obtained by employing the experimentally determined values of I_o, T, and $\ln r_c/r_o$ to compute the value of B_o and kT/e.

There is, of course, no means at this late date of interrogating the experimentalist

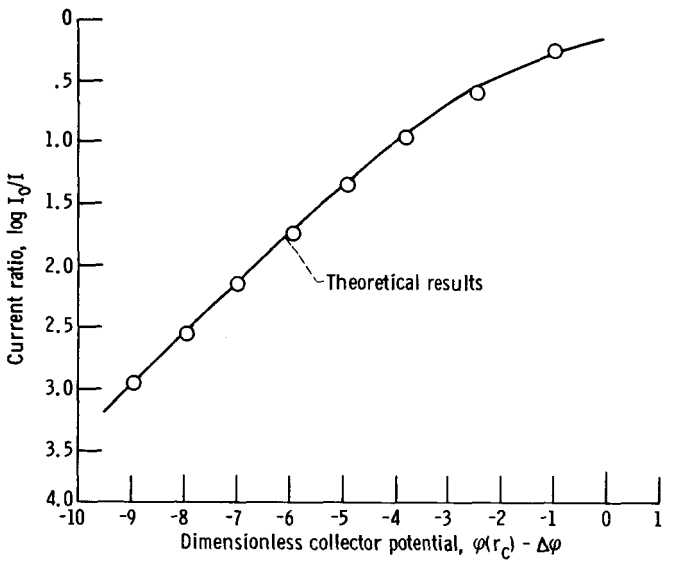

(a) Schottky (ref. 3). Run 1; collector radius, 56.

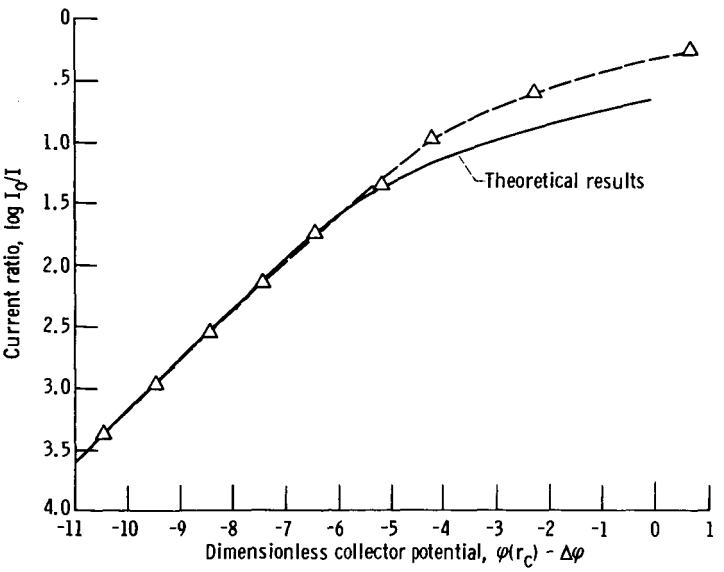

(b) Schottky (ref. 3). Run 2; collector radius, 56.

Figure 8. - Comparison with experiment.

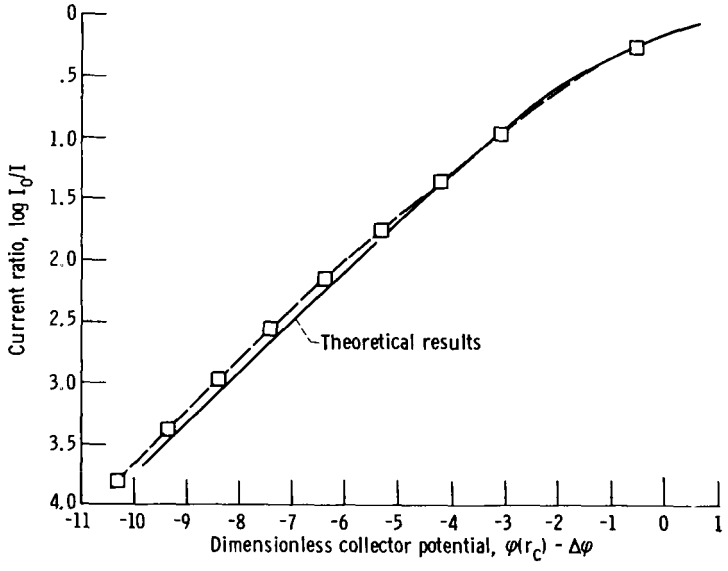

(c) Schottky (ref. 3). Run 8; collector radius, 30.

Figure 8. - Concluded.

to try to discover reasons for the discrepancies between theory and experiment. It is to be noted that Schottky also observed marked discrepancies between observed results which he could not satisfactorily explain. Of importance here, however, is that the entire theoretical current-voltage characteristic can be generated and compared with experiment. After perusing the theoretical current-voltage curves of figure 6, one might suspect that something had affected the experimental determination of B_0 in figure 8(b); while in figure 8(c) either $\hat{r}_c/\hat{r}_0$ or a combination of work function and B_0 might be suspect.

Further experimentation might also better define limitations of the model. For instance, just when it is no longer valid to neglect short range electron-electron interactions is still a moot point.

CONCLUSIONS

A complete formulation of the collisionless cylindrical diode with electron emission has been presented. The numerical solutions describe the physical characteristics of these diodes. It is now possible, by comparing theory with experiment over the whole current-voltage curve, to obtain a more detailed understanding of the cylindrical electron diode.

The analysis also shows that the onset of the Schottky retarding region for cylindrical diodes does not coincide, in general, with the onset of monotonically retarding potentials.

Lewis Research Center,
National Aeronautics and Space Administration,
Cleveland, Ohio, January 9, 1968,
129-02-01-05-22.

APPENDIX A

SYMBOLS

B_o	space-charge parameter (eqs. (B11) and (B12))
E	total energy in $\hat{r}, \theta$ plane (eq. (5))
I	electron current (eq. (1))
I_o	emitted (or saturation) electron current
k	Boltzmann constant (eq. (3))
L	angular momentum (eq. (4))
l	length of diode (eq. (B5))
m	electron mass (eq. (4))
n	electron density (eq. (B6))
P	parameter, space-charge integral (eq. (C30))
p	parameter, space-charge integral (eq. (B9))
Q	parameter, space-charge integral (eq. (C30))
q	parameter, space-charge integral (eq. (B10))
r	radial coordinate (eq. (4))
S	space-charge integral (eq. (C1))
T	emitter temperature (eq. (B3))
u	radial velocity component (eq. (B3))
$\bar{u}_o, \underline{u}_o$	upper and lower limits of integration over u_o (eq. (B7))
u_τ	thermal velocity (eq. (B3))
V	potential energy
v	aximuthal velocity component (eq. (B3))
w	axial velocity component (eq. (B3))
z	axial coordinate (eq. (B1))
ϵ_o	vacuum permittivity (mks units) (eq. (B12))
η	parameter (eq. (B3))
θ	aximuthal coordinate (eq. (B1))
ξ	transformed coordinate (eq. (B13))
φ	dimensionless potential (eqs. (1) to (3))
φ_c	collector potential
φ_{cm}	collector potential for potential with zero slope at collector
φ_{sat}	collector potential for potential with zero slope at emitter
φ_{sch}	collector potential for first potential in SRR

Subscripts:

e	envelope, Wheatcroft plots
m	potential minimum
max	maximum value
min	minimum value

Superscript:

^	dimensional variable

APPENDIX B

MATHEMATICAL FORMULATION

Except for notation, this appendix reiterates appendix 1 in Wheatcroft's paper (ref. 2). All symbols are defined in appendix A.

Motion of Electrons in Cylindrical Geometry

The coordinate system to be employed is depicted in figure 9. The velocity components are given by

$$\left.\begin{aligned} \hat{u} &= \frac{d\hat{r}}{dt} \\ \hat{v} &= \frac{\hat{r}\, d\theta}{dt} \\ \hat{w} &= \frac{d\hat{z}}{dt} \end{aligned}\right\} \tag{B1}$$

In this system, the dimensionless radial velocity component u(r) satisfies the equation

$$u^2(r) = \varphi(r) + u_o^2 + \eta v_o^2 \tag{B2}$$

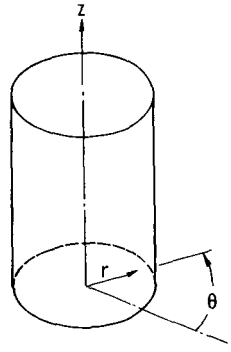

Figure 9. - Cylindrical coordinate system.

where

$$\left.\begin{aligned} u &\equiv \frac{\hat{u}}{\hat{u}_\tau} \\ v &\equiv \frac{\hat{v}}{\hat{u}_\tau} \\ r &\equiv \frac{\hat{r}}{\hat{r}_o} \\ \eta &\equiv 1 - r^{-2} \\ \hat{u}_\tau &\equiv \sqrt{\frac{2kT}{m}} \end{aligned}\right\} \tag{B3}$$

and the subscript o refers to conditions at $\hat{r} = \hat{r}_o$ (r = 1).

With this notation, the Maxwellian velocity distribution function of the emitted current I can be written as

$$dI = \frac{2I_o}{\pi}\, u_o e^{-\left(u_o^2+v_o^2+w_o^2\right)} du_o\, dv_o\, dw_o \tag{B4}$$

where, as in equations (B3), $w \equiv \hat{w}/\hat{u}_\tau$.

Electron Space Charge

The contribution to the dimensionless electron density $n(r) = \hat{n}(r)/\hat{n}_o$ of dI reaching r is given by (after integrating over w_o from $-\infty$ to ∞)

$$dn(r) = \frac{2}{\pi l}\, \frac{u_o\, e^{-\left(u_o^2+v_o^2\right)}}{r u(r)}\, du_o\, dv \tag{B5}$$

where n_o is the density of emitted electrons given by

$$n_o = \frac{I_o}{2\pi r_o l} \frac{\sqrt{\pi}}{eu_\tau} \tag{B6}$$

and $u(r)$ is given by equation (B1).

Integrating over u_o, v_o results in

$$\eta(r) = \frac{2}{\pi r} \int_{-\infty}^{\infty} dv_o \int_{\underline{u}_o}^{\bar{u}_o} \frac{u_o \, e^{-\left(u_o^2 + v_o^2\right)}}{u(r)} du_o \tag{B7}$$

It should be noted that contributions to the density $n(r)$ at any radius r will result from electrons flowing to the collector as well as electrons returning to the emitter. These various contributions are implicit in the limits of equation (B7). Their unique formulations are presented in appendixes C and D where $\bar{u}_o$ and $\underline{u}_o$ are explicitly defined in terms of v_o.

The integration over du_o in equation (B7) may be performed in closed form by first transforming the variable of integration to $u(r)$ (eq. (B2)):

$$n(r) = \frac{e^{\varphi(r)}}{r\sqrt{\pi}} \int_{-\infty}^{\infty} e^{-r^{-2}v_o^2} \left(\operatorname{erf} p - \operatorname{erf} q\right) dv_o \tag{B8}$$

$$p^2 \equiv \bar{u}_o^2 + \eta v_o^2 + \varphi(r) \tag{B9}$$

$$q^2 \equiv \underline{u}_o^2 + \eta v_o^2 + \varphi(r) \tag{B10}$$

Poisson's Equation

Poisson's equation in dimensionless form for the cylindrical case becomes

$$\frac{1}{r} \frac{d}{dr} \left(r \frac{d\varphi}{dr} \right) = B_o \, n(r) \tag{B11}$$

where B_o (in mks units) is

$$B_o \equiv \frac{e^2 n_o r_o^2}{\epsilon_o kT} \tag{B12}$$

and ϵ_o is the permittivity of free space. Employing the transformation,

$$\xi \equiv \ln r \tag{B13}$$

Poisson's equation (B11) can then be expressed as

$$\varphi''(\xi) = B_o\, e^{2\xi}\, n(\xi, \varphi) \tag{B14}$$

where the primes denote differentiation with respect to ξ. In terms of ξ, equations (B8), (B9), and (B10) become

$$n(\xi, \varphi) = \frac{e^{\varphi(\xi)}}{\sqrt{\pi}} \int_{-\infty}^{\infty} e^{-z^2} (\text{erf } p - \text{erf } q)\, dz \tag{B15}$$

where

$$z \equiv v_o\, e^{-\xi} \tag{B16}$$

and

$$p^2 = \overline{u}_o^2 + (e^{2\xi} - 1)z^2 + \varphi(\xi) \tag{B17}$$

$$q^2 = \underline{u}_o^2 + (e^{2\xi} - 1)z^2 + \varphi(\xi) \tag{B18}$$

APPENDIX C

RETARDING FIELD

Space-Charge Integral

Although the numerical solutions will ultimately be performed by employing the independent variable ξ and equations (B14) to (B18), in this section the independent variable r (eqs. (B8) to (B10)) will be used purely for notational convenience and clarity because it precludes the need for writing the troublesome and nonpysical e^{ξ} for r. Furthermore, it will be convenient to define a factor S such that

$$n(r) = \frac{2e^{\varphi(r)}}{r\sqrt{\pi}} S(r) \tag{C1}$$

or

$$S = \int_0^{\infty} e^{-v_o^2/r^2} (\operatorname{erf} p - \operatorname{erf} q) dv_o \tag{C2}$$

and from equation (B10),

$$\left.\begin{aligned} p^2 &\equiv \bar{u}_o^2 + \eta v_o^2 + \varphi(r) \\ q^2 &\equiv \underline{u}_o^2 + \eta v_o^2 + \varphi(r) \end{aligned}\right\} \tag{C3}$$

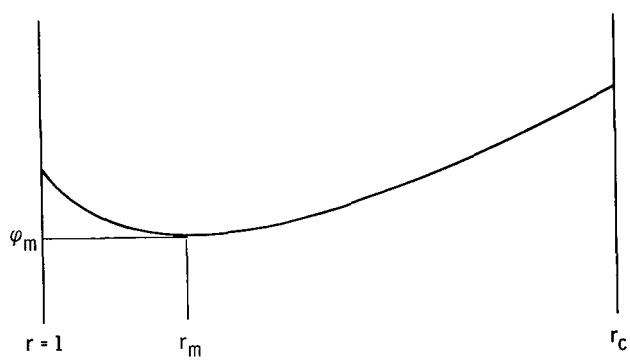

Figure 10. - Typical potential.

A typical dimensionless potential distribution is shown in figure 10 (note by definition of φ, V_{max} corresponds to φ_{min}). The retarding region of this potential is specified by $r < r_m$. It is now necessary to determine the limits $\overline{u}_o^2$ and $\underline{u}_o^2$. They will, in general, be functions of v_o.

Case 1: Wheatcroft Case

The relation between u_o^2 and v_o^2 is most easily seen by a Wheatcroft plot. The actual plot employed by Wheatcroft (ref. 2, fig. 7) is shown in figure 11 with the notation

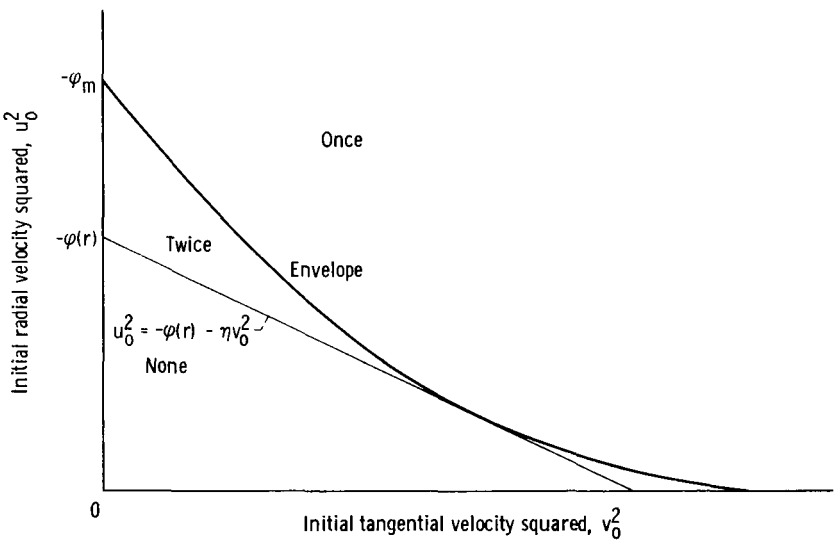

Figure 11. - Wheatcroft plot.

of the present report. Before discussing the interpretation of the Wheatcroft plot, it will be helpful to describe its derivation. From equation (B2), the radial velocity at any r of an electron emitted with initial velocity components u_o and v_o is given by

$$u^2(r) = u_o^2 + \eta v_o^2 + \varphi(r) \tag{C4}$$

If a given electron (i.e., a given ordered pair (v_o^2, u_o^2)) reaches a given radius r, its radial velocity there must be greater than or equal to zero. Setting $u^2(r) = 0$ in equation (C4) results in a linear relation between u_o^2 and v_o^2:

$$u_o^2 = -\varphi(r) - \eta(r) v_o^2 \tag{C5}$$

The locus of points (v_o^2, u_o^2) satisfying equation (C5) is drawn in figure 11. None of the electrons whose ordered pairs (v_o^2, u_o^2) lie below this line can reach radius r. The converse is not true, as shown in the next paragraph.

In figure 12 equation (C5) has been plotted for two radii. The line labeled r_m corresponds to the location of φ_m. As described previously, none of those electrons with ordered pairs (v_o^2, u_o^2) in the region defined by $u_o^2 = 0$, $v_o^2 = 0$, and $u_o^2 < -\varphi(r_m) - \eta(r_m)v_o^2$ will reach r_m. Neither will <u>all</u> the electrons lying outside this region reach r_m. In fact, the shaded area in the figure shows a group of electrons out-

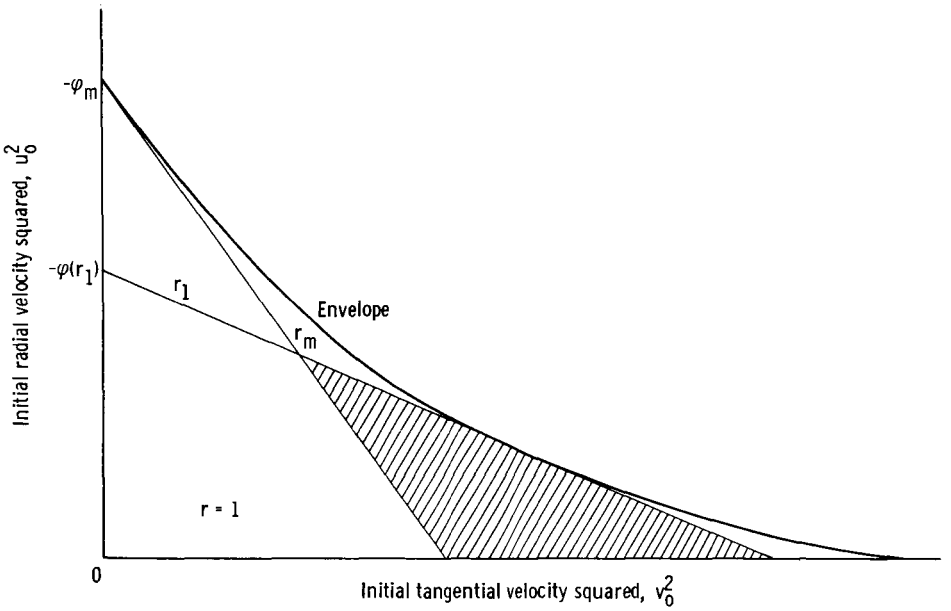

Figure 12. - Construction of Wheatcroft plot.

side this region which do not reach $r_1 < r_m$. This is portrayed in a different manner by the EODP given in figure 3(a). There the critical potential energy was not V_{max} but $\tilde{V}_{max}$; generally $\tilde{V}_{max}$ occurs at a smaller radius than V_{max}. The correlation between figure 3(a) and figure 12 can best be understood by noting that a given v_o^2 in figure 12 corresponds to a particular V_L in figure 3(a). Increasing u_o^2 in figure 12 corresponds to an increase in E in figure 3(a).

The curve in figure 12 is simply the envelope of the curves in equation (C5) for $r_o \leq r \leq r_m$. All electrons with (v_o^2, u_o^2) outside this envelope reach the collector, or, equivalently, all electrons with (V_L, E) so that $E > \tilde{V}_{max}$ in figure 3(a) will reach the collector.

The equation for the envelope $(v_e^2, u_e^2) = 0$ can be derived in parametric form from equation (C5) by the usual method to give

$$v_e^2(t) = -\frac{t^3\varphi'(t)}{2} \qquad 1 \le t \le r_m \tag{C7a}$$

and

$$u_e^2(t) = -\varphi(t) - \eta(t)v_e^2 \qquad 1 \le t \le r_m \tag{C7b}$$

$$\left(v_e^2, u_e^2\right)_{t=r_m} = (0, -\varphi_m) \tag{C8a}$$

$$\left(v_e^2, u_e^2\right)_{t=1} = \left(\frac{-\varphi'(1)}{2}, 0\right) \tag{C8b}$$

(the Wheatcroft case (ref. 2) explicitly requires the existence of a potential minimum in the interelectrode space).

From equations (C2) and (C3), the minimum radial velocity u_o^2 at the emitter such that an electron will reach radius r is (see fig. 11)

$$\left.\begin{aligned} \underline{u}_o^2 &= -\varphi(r) - \eta(r)v_o^2 \qquad 0 \le v_o \le v_e(r) \\ \underline{u}_o^2 &= u_e^2\left(v_o^2\right) \qquad v_e(r) < v_o < \infty \end{aligned}\right\} \tag{C9}$$

The maximum radial velocity for electrons passing radius r once is

$$\overline{u}_o^2 = \infty \qquad 0 \le v_o \le \infty \tag{C10a}$$

and for electrons passing radius r twice is

$$\overline{u}_o^2 = u_e^2\left(v_o^2\right) \qquad 0 \le v_o \le v_e(r) \tag{C10b}$$

Substituting equations (C9) and (C10) into equation (C3) results in, for electrons passing radius r once,

$$\operatorname{erf} p = 1 \qquad 0 \le v_o \le \infty \tag{C11a}$$

and for electrons passing radius r twice,

$$\operatorname{erf} p = \operatorname{erf} p_e \qquad 0 \le v_o \le v_e(r) \tag{C11b}$$

$$\operatorname{erf} q = 0 \qquad 0 \le v_o \le v_e(r) \tag{C12a}$$

$$\operatorname{erf} q = \operatorname{erf} p_e \qquad v_e(r) < v_o < \infty \tag{C12b}$$

where

$$p_e^2 = u_e^2\left(v_o^2\right) + \eta(r)v_o^2 + \varphi(r) \tag{C13}$$

Substituting equations (C11) to (C13) into equation (C2) results in

$$S_1(r) = \int_0^\infty e^{-v_o^2/r^2}\, dv_o + \int_0^{v_e(r)} e^{-v_o^2/r^2} \operatorname{erf} p_e\, dv_o - \int_{v_e(r)}^\infty e^{-v_o^2/r^2} \operatorname{erf} p_e\, dv_o \qquad r \le r_m$$

or

$$S_1(r) = r\frac{\sqrt{\pi}}{2} + \int_0^{v_e(r)} e^{-v_o^2/r^2} \operatorname{erf} p_e\, dv_o - \int_{v_e(r)}^\infty e^{-v_o^2/r^2} \operatorname{erf} p_e\, dv_o \qquad r \le r_m \tag{C14}$$

where the subscript 1 refers to case 1, and $v_e^2(r)$ is, from equation (C7a),

$$v_e^2(r) = -\frac{r^3\varphi'(r)}{2} \tag{C15}$$

Case 2: Modified Wheatcroft Case

Wheatcroft (ref. 2) considered only the situation where $r_m \le r_c$ (radius of the collector). The situation that exists when the potential is monotonically decreasing with negative slope at the collector is a simple extension which can be completely described by reference to figure 13. Here the envelope $\left[v_e^2(t),\ u_e^2(t)\right] = 0$ proceeds in the same way as in case 1 from $t = 1$ to $t = r_c$. Then, however, it deviates from the previous case (dashed curve in fig. 13) and proceeds along the straight line defined by

$$u_o^2 = -\varphi(r_c) - \eta(r_c)v_o^2$$

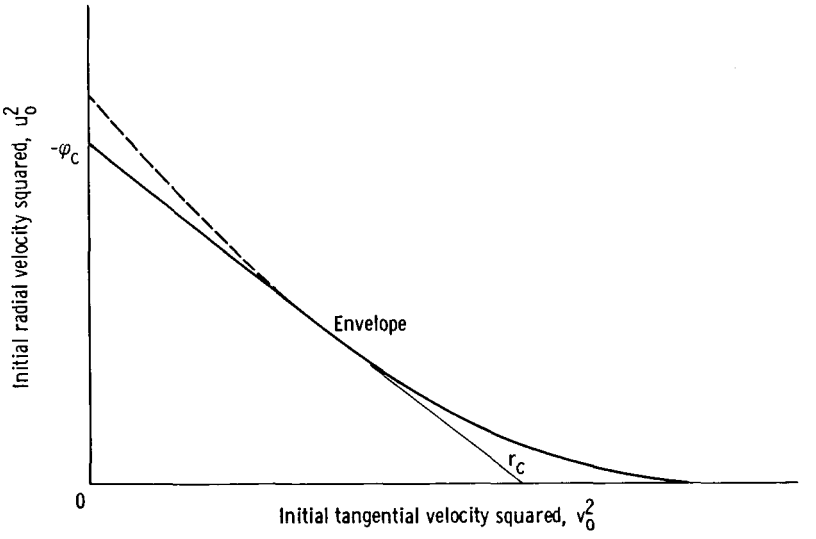

Figure 13. - Modified Wheatcroft plot.

Hence, the only change in analysis for case 1 is an obvious modification to the definition of the envelope, equation (C7).

Case 3: Effective Accelerating Field for $r_0 \leq r \leq r_m$

Case 3 can be defined by either figure 14 or the EODP of figure 4(b). Figure 3(a) shows that case 1 tacitly assumes a net retarding field at the emitter. This is most easily observed by noting the slope of $\tilde{V}$ at r_o; a positive slope implies a retarding field and vice versa. Figure 4(b), however, shows case 3 to have an accelerating field in front of the emitter.

The only physically meaningful region in figure 14 is that for which $v_o^2 > 0$, $u_o^2 > 0$. The point $\left(v_o^2, u_o^2\right) = \left(v_1^2, 0\right)$ indicated in this figure corresponds to r_1 in figure 4(b); that is, an electron emitted with $E = 0$ and $L = r_o v_1$ will reach radius r_1 before being reflected by $\tilde{V}$ to the emitter.

Figure 14 implies a collector potential φ_c well within the SRR, for it is readily apparent that any electron with emitted velocities such that $\left(v_o^2, u_o^2\right)$ lies on or above the line labeled r_c will reach the collector.

For this case, where $r = r_1$

$$\underline{u}_o^2 = -\varphi(r_1) - \eta(r_1)v_o^2 \qquad 0 \leq v_o \leq v_1$$

$$\underline{u}_o^2 = 0 \qquad v_1 \leq v_o \leq \infty$$

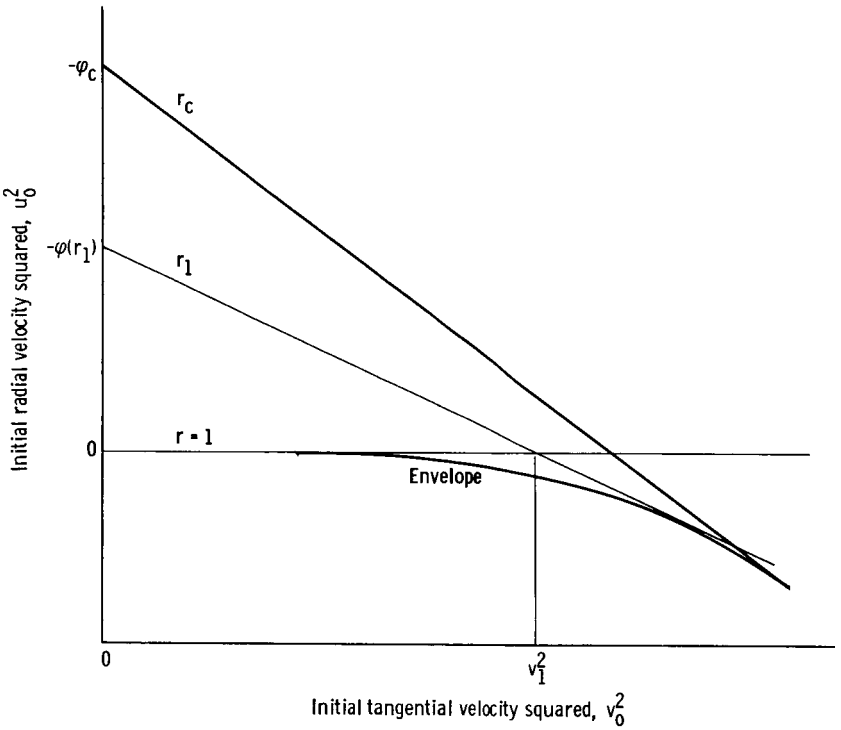

Figure 14. - Wheatcroft plot: effective accelerating region.

and for electrons passing r_1 once,

$$\bar{u}_o^2 = \infty \qquad 0 \le v_o \le \infty$$

and for electrons passing r_1 twice,

$$\bar{u}_o^2 = -\varphi(r_c) - \eta(r_c)\, v_o^2 \qquad 0 \le v_o \le v_c$$

Hence, for electrons passing r_1 once

$$\text{erf } p = 1 \qquad 0 \le v_o \le \infty$$

for electrons passing r_1 twice

$$\text{erf } p = \text{erf } p_c \qquad 0 \le v_o \le v_c$$

$$\text{erf } q = 0 \qquad 0 \le v_o \le v_1$$

$$\text{erf } q = \text{erf } q_c \qquad v_1 \le v_o \le \infty$$

and

$$S_3(r_1) = \frac{r_1\sqrt{\pi}}{2} + \int_0^{v_c} e^{-v_o^2/r_1^2} \operatorname{erf} p_c - \int_{v_1}^{\infty} e^{-v_o^2/r^2} \operatorname{erf} q_c \tag{C18}$$

$$\left.\begin{aligned} p_c^2 &\equiv \left[\eta(r_1) - \eta(r_c)\right] v_o^2 + \varphi(r_1) - \varphi(r_c) \\ q_c^2 &\equiv \eta(r_1) v_o^2 + \varphi(r_1) \end{aligned}\right\} \tag{C19}$$

where from equation (C5) for $u_o^2 = 0$,

$$\left.\begin{aligned} v_c^2 &= -\frac{\varphi(r_c)}{\eta(r_c)} \\ v_1^2 &= -\frac{\varphi(r_1)}{\eta(r_1)} \end{aligned}\right\} \tag{C20}$$

General Case for Monotonically Retarding Potentials

Between cases 1, 2, and 3 there are a number of cases which are merely variations on the same theme. Rather than describe all possible cases individually, the equations of a general situation will be defined. It will then be shown how these equations may be easily specialized to represent all possible cases.

The EODP for the general case is shown in figure 3(d). The Wheatcroft plot is shown in figure 15. In this figure, the envelope of interest is given by the implicit equations

$$\left[v_1^2(t),\ u_1^2(t)\right] = 0 \qquad 1 \le t \le r_a \tag{C21a}$$

$$\left[v_2^2(t),\ u_1^2(t)\right] = 0 \qquad r_b \le t \le r_m \tag{C21b}$$

Let v_r^2 be defined by the point of tangency between the envelope and equation (C5). Then for r such that $v_x^2 < v_r^2$, figure 15 can be represented by figure 16 where the envelope $\left(v_e^2, u_e^2\right) = 0$ is given by

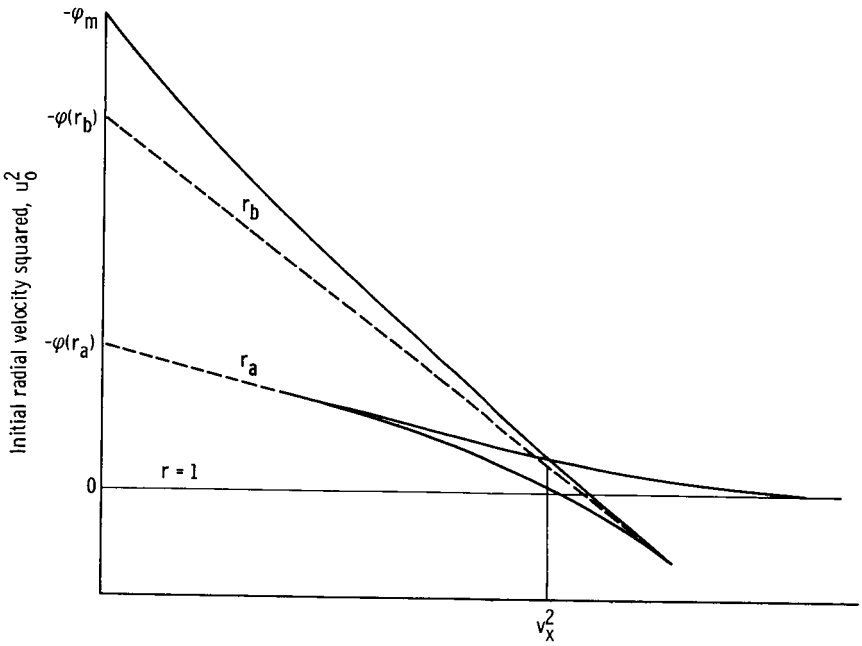

Figure 15. - Wheatcroft plot: general case.

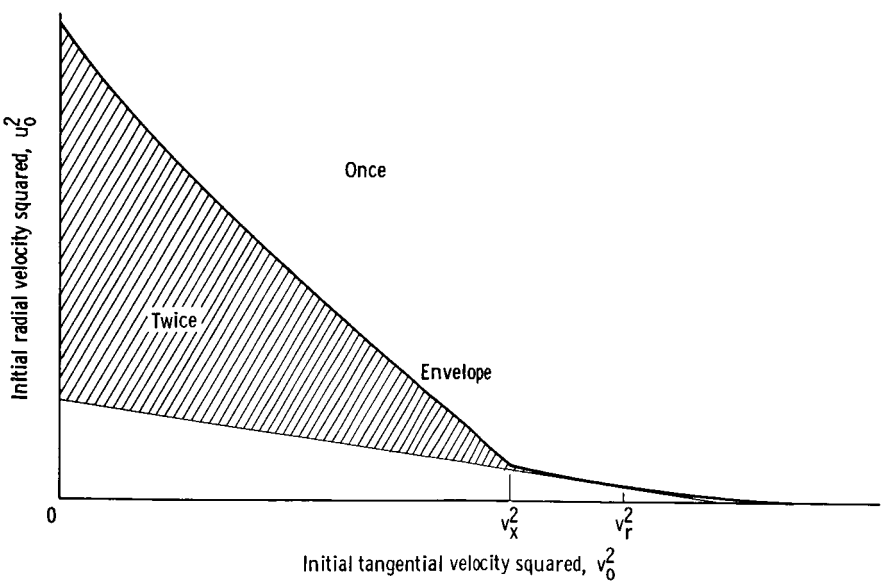

Figure 16. - General case: regime 1.

$$\left(v_e^2, u_e^2\right) \equiv \left(v_1^2, u_1^2\right) = 0 \qquad v_o > v_x$$

$$\left(v_e^2, u_e^2\right) \equiv \left(v_2^2, u_2^2\right) = 0 \qquad 0 < v_o < v_x \tag{C22}$$

Now figure 16, with the envelope defined by equation (C22), represents the same situation as figure 11, case 1. Hence, from case 1,

$$S(r) = \frac{r\sqrt{\pi}}{2} + \int_0^{v_e(r)} e^{-v_o^2/r^2} \operatorname{erf} p_e \, dv_o - \int_{v_e(r)}^{\infty} e^{-v_o^2/r^2} \operatorname{erf} p_e \, dv_o \qquad \underline{v_e(r) > v_x} \tag{C23}$$

and p_e is given by equation (C13).

The next region of interest (see fig. 15) is that for which $v_e(r) = v_1(r) < v_x$ and

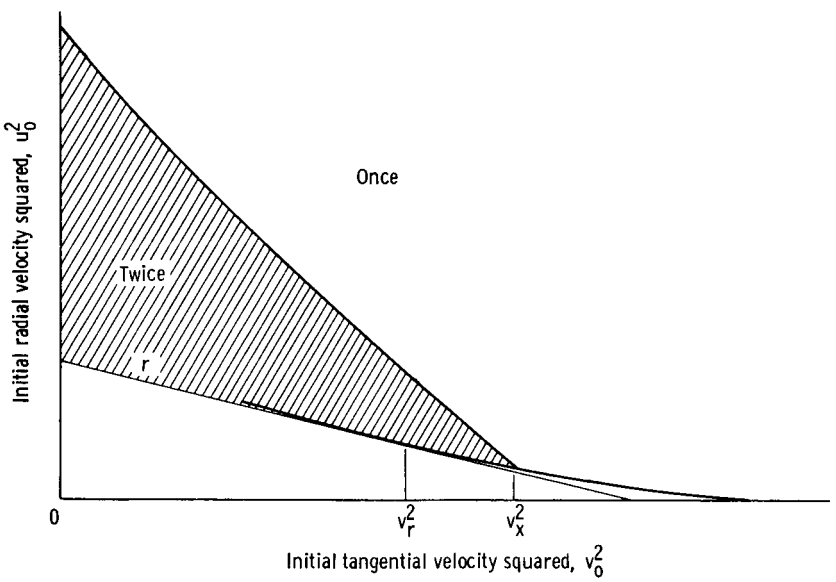

Figure 17. - General case: regime 2.

$r < r_a$. The Wheatcroft plot for this case is shown in figure 17. Hence,

$$\underline{u_o^2} = -\varphi(r) - \eta(r)v_o^2 \qquad 0 \le v_o \le v_r$$

$$\underline{u_o^2} = u_1^2\left(v_o^2\right) \qquad v_o \ge v_r$$

for electrons passing r once,

$$\bar{u}_o^2 = \infty \qquad 0 \le v_o \le \infty$$

for electrons passing r twice,

$$\bar{u}_o^2 = u_2^2(v_o^2) \qquad 0 \le v_o \le v_x$$

and for electrons passing r once,

$$\text{erf } p = 1 \qquad 0 \le v_o \le \infty \tag{C24a}$$

for electrons passing r twice

$$\text{erf } p = \text{erf } p_e \qquad 0 \le v_o \le v_x \tag{C24b}$$

$$\left.\begin{aligned} \text{erf } q &= 0 \qquad 0 \le v_o \le v_r \\ \text{erf } q &= \text{erf } q_1 \qquad v_o \ge v_r \end{aligned}\right\} \tag{C25}$$

where p_e is given by equation (C13) since $u_2(r) = u_e(r)$ of equation (C22) in the range $0 \le v_o \le v_x$, and

$$q_1^2 = u_1^2(r) + \eta(r)v_o^2 + \varphi(r) \tag{C26}$$

The space-charge integral for this region then becomes

$$S(r) = \frac{r\sqrt{\pi}}{2} + \int_0^{v_x} e^{-v_o^2/r^2} \text{erf } p_e \, dv_o - \int_{v_r}^{v_x} e^{-v_o^2/r^2} \text{erf } q_1 dv_o$$

$$- \int_{v_r}^{\infty} e^{-v_o^2/r^2} \text{erf } q_1 \, dv_o \qquad \underline{v_r < v_x, \; r < r_a} \tag{C27}$$

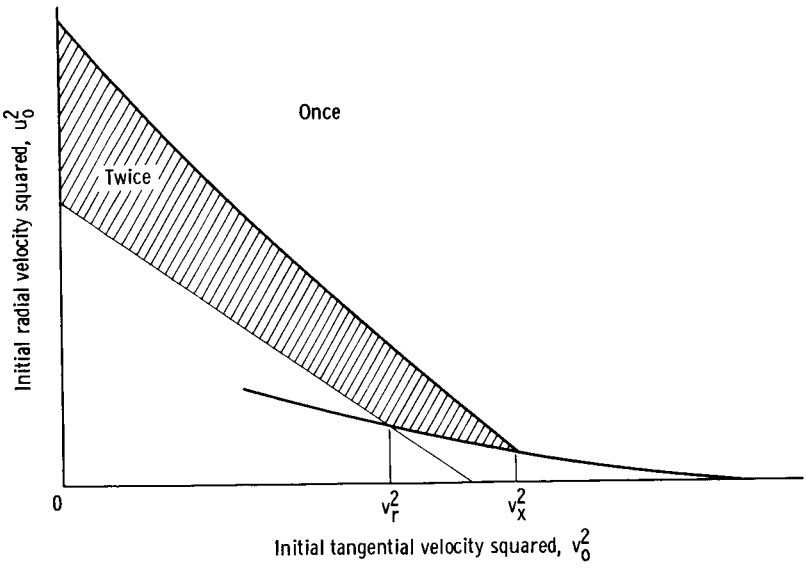

Figure 18. - General case: regime 3.

Regime 3 is shown in figure 18; for this regime

$$\underline{u}_o^2 = -\varphi(r) - \eta(r)v_o^2 \qquad 0 < v_o < v_r$$

$$\underline{u}_o^2 = u_1^2(r) \qquad v_o > v_r$$

for electrons passing r once,

$$\overline{u}_o^2 = \infty \qquad 0 \leq v_o \leq \infty$$

for electrons passing r twice,

$$\overline{u}_o^2 = u_2^2(r) \qquad 0 \leq v_o \leq v_x$$

for electrons passing r once,

$$\text{erf } p = 1 \qquad 0 \leq v_o \leq \infty$$

for electrons passing r twice,

$$\text{erf } p = \text{erf } p_e \qquad 0 \leq v_o \leq v_x$$

$$\text{erf } q = 0 \qquad 0 < v_o < v_1$$

$$\text{erf } q = \text{erf } q_1 \qquad v_o > v_r$$

and

$$S(r) = \frac{r\sqrt{\pi}}{2} + \int_0^{v_x} e^{-v_o^2/r^2} \text{ erf } p_e \, dv_o - \int_{v_r}^{v_x} e^{-v_o^2/r^2} \text{ erf } q_1 \, dv_o$$

$$- \int_{v_r}^{\infty} e^{-v_o^2/r^2} \text{ erf } q_1 \, dv_o \qquad \underline{v_r < v_x, \; r > r_a} \qquad \text{(C28)}$$

where p_e is given by equation (C13) and q_1 by equation (C26).

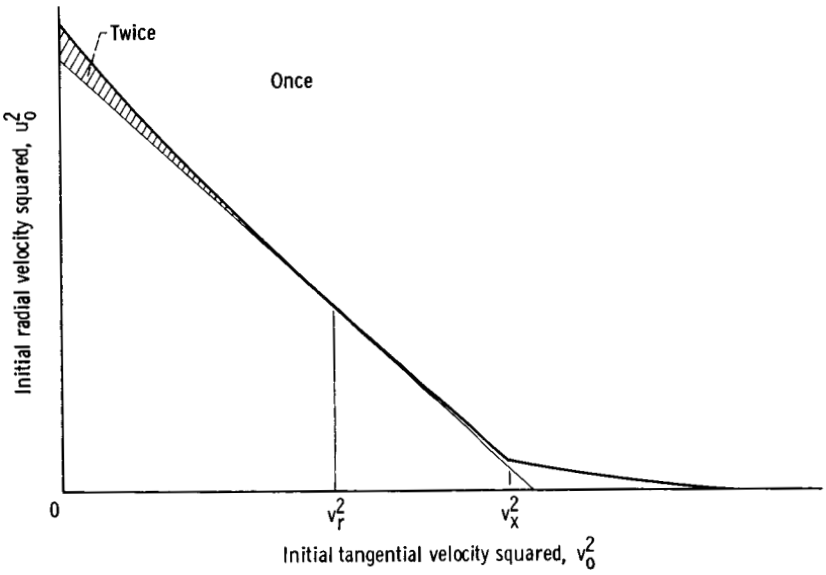

Figure 19. - General case: regime 4.

The final regime of interest in the general case is shown in figure 19. The analysis of this regime is identical to that of regime 1 (fig. 16). Hence, from equations (C13) and (C20) to (C23)

$$S(r) = \frac{r\sqrt{\pi}}{2} + \int_0^{v_e(r)} e^{-v_o^2/r^2} \text{ erf } p_e \, dv_o - \int_{v_e(r)}^{\infty} e^{-v_o^2/r^2} \text{ erf } p_e \, dv_o \qquad \underline{v_e(r) < v_x} \qquad \text{(C29)}$$

The space-charge integral for the general case, equations (C13) and (C20) to (C28) may be put in the following more concise form:

$$S(r) = \frac{r\sqrt{\pi}}{2} + 2\int_0^B P\,dv_o - \int_0^\infty P\,dv_o - \int_A^B Q\,dv_o \tag{C30}$$

$$\left.\begin{aligned} P^2 &\equiv e^{-v_o^2/r^2}\ \operatorname{erf}\left[u_e^2(r) + \eta(r)v_o^2 + \varphi(r)\right] \\ Q^2 &\equiv e^{-v_o^2/r^2}\ \operatorname{erf}\left[u_1^2(r) + \eta(r)v_o^2 + \varphi(r)\right] \end{aligned}\right\} \tag{C31}$$

$$\left.\begin{aligned} v_i^2(t) &= -\frac{t^3\varphi'(t)}{2} \\ u_i^2(t) &= -\varphi(t) - \eta(t)v_i^2(t) \end{aligned}\right\} \tag{C32}$$

where $i = 1$ for $1 \le t \le r_a$, and $i = 2$ for $r_b \le t \le r_m$,

$$\left.\begin{aligned} \left(v_e^2, u_e^2\right) &\equiv \left(v_1^2, u_1^2\right) \qquad v_1 > v_x \\ \left(v_e^2, u_e^2\right) &\equiv \left(v_2^2, u_2^2\right) \qquad v_2 < v_x \end{aligned}\right\} \tag{C33}$$

and the limits A and B are defined in table I. Note that from (C32), $v_r^2 = -\left[r^3\varphi'(r)\right]/2$.

The Wheatcroft case (case 1) corresponds to $v_x = 0$. Case 3 is obtained for $r_a = r_o$ with $u_1 = 0$, $0 \le v_o \le \infty$.

TABLE I. - LIMITS A AND B OF SPACE-CHARGE INTEGRAL

Regime	Criteria	A	B
1	$v_r > v_x$	v_r	v_r
2	$v_r < v_x$, $r < r_a$	v_r	[a] v_x
3	$v_r < v_x$, $r > r_a$	[b] $v_{int}(r)$	v_x
4	$v_r < v_x$	v_r	v_r

[a] Intersection point between $v_1(t)$ and $v_2(t)$.

[b] Intersection point between $u_o^2 = -\varphi(r) - \eta(r)v_o^2$ and $u_1^2 = u_1^2(r)$.

General Case for $r_c < r_m$

After modifying $v_2(t)$ (eq. (C32)) as indicated in case 2, equations (C30) then (C33) with table I represent the most general situation.

Current to Collector

To obtain the current to the collector, it is only necessary to integrate equation (B4) along the envelope $\left(v_e^2, u_e^2\right)$ of the generalized Wheatcroft plot figure 15 (after integrating over dw_o):

$$\frac{I}{I_o} = \frac{1}{\sqrt{\pi}} \int_{-\infty}^{\infty} e^{-u_e^2 v_o^2} dv_o \tag{C34}$$

APPENDIX D

ACCELERATING FIELD

An accelerating field is present for $r > r_m$ (see fig. 10). The Wheatcroft plot for the general case ($r_m \leq r_c$) is shown in figure 20.

The analysis is the same as that for a retarding field with

$$\underline{u}_o^2 = u_e^2\left(v_o^2\right)$$

$$\overline{u}_o^2 = \infty$$

where $u_e^2 = u_e^2\left(v_e^2\right)$ is defined by equation (C32) in the general case. Hence,

$$S(r) = \frac{r\sqrt{\pi}}{2} - \int_0^\infty e^{-v_o^2/r^2} \operatorname{erf} q\left(v_o^2\right) dv_o \tag{D1}$$

where

$$q^2 = u_e^2\left(v_o^2\right) + \eta(r)v_o^2 + \varphi(r) \tag{D2}$$

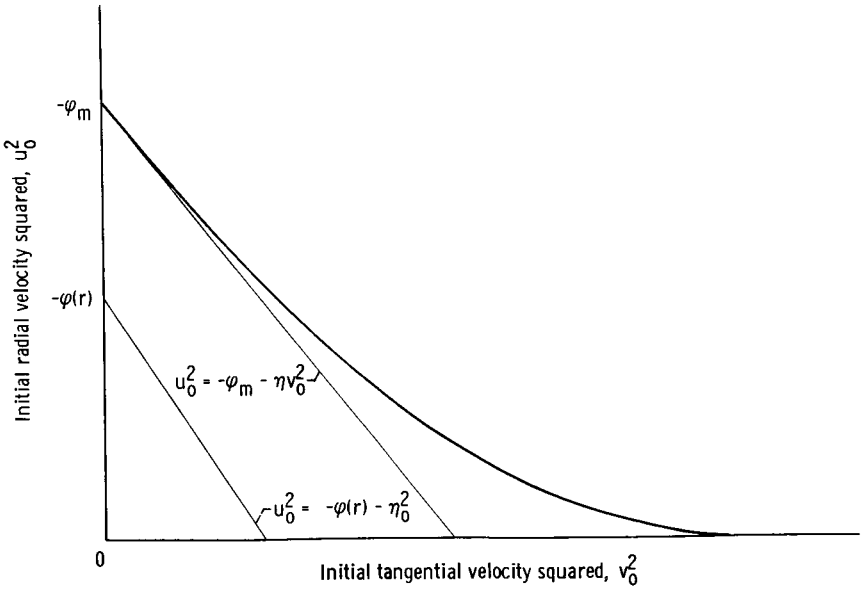

Figure 20. - Wheatcroft plot for accelerating region.

REFERENCES

1. Ivey, Henry F.: Space Charge Limited Currents. Advances in Electronics and Electron Physics. Vol. 6. Academic Press, 1954, pp. 137-256.

2. Wheatcroft, E. L. E.: The Theory of the Thermionic Diode. Inst. Elect. Eng. J., vol. 86, no. 521, May 1940, pp. 473-484.

3. Schottky, W.: Emission of Electrons from an Incandescent Filament Under the Action of a Retarding Potential. Ann. d. Physik, vol. 44, no. 7, July 17, 1914, pp. 1011-1032.

4. Nottingham, W. B.: Thermionic Emission. Handbuch der Physik. Vol. 21. S. Flugge, ed., Springer-Verlag (Berlin), 1956, pp. 1-231.

5. Langmuir, I.: The Effect of Space Charge and Initial Velocities on the Potential Distribution and Thermionic Current Between Parallel Plane Electrodes. Phys. Rev., vol. 21, no. 4, Apr. 1923, pp. 419-435; see also Suits, C. G., ed.: The Collected Works of I. Langmuir. Vol. 3. Pergammon Press, 1961, pp. 95-110.

6. Goldstein, Herbert: Classical Mechanics. Addison-Wesley Press, 1950, p. 63.

NASA-Langley, 1968 —— 10 E-4065